Table 3
Feature of wound dehiscence and clinical outcome of patients with it

Pt	Age at Op	Performed Op	Day at onset of WD	Day of strating NPWT	Day of starting Arginaid	Bacterias associated to WD	Area of WD	Depth of WD	Days for closure of WD
1	26 MO	Laryngotracheal separation	POD-7	POD-11	POD-11	Pseudomonas aeruginosa	Neck (4.4 × 1.7 cm)	1.7 cm	18 days
2	0 DO	Radical op for spinal bifida	POD-12	POD-12	POD-22	MSSA Klebsiella	Sacral area (5.5 × 3.8 cm)	2.4 cm	32 days
3	31 MO	Gastrostomy	POD-8	POD-11	POD-12	MRSA	Abdomen (3.6 × 2.5 cm)	1.0 cm	14 days
4	6 MO	Reconstruction of colostomy	POD-7	POD-7	POD-7	MRSA Pseudomonas aeruginosa	Abdomen (4.3 × 2.5 cm)	1.8 cm	17 days
5	10 MO	Anorectoplasty	POD-8	POD-8	POD-8	Pseudomonas aeruginosa	Sacral and perineal area (6.0 × 2.8 cm)	2.2 cm	26 days
6	1 DO	Tumor extirpation	POD-4	POD-5	POD-5	Pseudomonas aeruginosa	Sacral and perineal area (4.8 × 3.4 cm)	1.7 cm	28 days

Abbreviations: B, boy; DO, day old; G, girl; MO, month old; MSSA, Methicillin-sensitive Staphylococcus aureus; MRSA, Methicillin-resistant Staphylococcus aureus; NPWT, negative pressure wound therapy; Op, operation; POD, postoprative day; WD, wound dehiscence.

There were no complications associated with this combination therapy during the therapy and observation periods after discontinuing the combination therapy.

Chronological change in blood plasma arginine concentration

The therapeutic level of plasma arginine in blood before combination therapy was below the normal range (44.0 ± 14.3 nmol/mL, normal range 53.6–133.6 nmol/mL). The mean arginine level showed a sufficient increase 1 to 4 wk after starting this therapy. The blood plasma arginine levels at 1 to 4 wk of therapy were 75.4 ± 16.6, 87.0 ± 15.5, 91.1 ± 16.4, and 90.2 ± 15.2 nmol/mL, respectively. The level of arginine during the therapeutic period was within the normal range. In addition, a significant difference was observed in the blood arginine level between the pre- and post-therapeutic investigation points ($P < 0.05$).

Discussion

The NPWT was developed for wound dehiscence with or without SSI and has been used extensively [5–12]. This therapy involves the insertion of an open-cell foam sponge into the wound, which is then sealed with an adhesive drape, and negative, subatmospheric pressure is applied, usually at 100 to 125 mmHg [5]. NPWT is generally thought to promote wound healing by removing local edema, which improves vascular and lymphatic flow, decreasing bacteria density, promoting angiogenesis in the wound, and increasing the formation of granulation tissue [7,11]. There have been several reports describing the advantages of NPWT for wound management in adult patients in the plastic and general surgical, thoracic, and orthopedic fields [5–12]. In contrast, there have been few reports of NPWT for wound management in pediatric patients after surgery [8–12]. Mooney et al. [8] treated 27 children with traumatic and infectious lower extremity tissue loss using NPWT. They applied the NPWT to acute and chronic wounds in their patients and reported that one-third of their patients had delayed primary wound closure or complete healing without the need for flap closure. Caniano et al. [9] also used NPWT in 51 pediatric surgical patients, including 12 patients with surgical wound dehiscence, and reported that NPWT was a safe and effective alternative to traditional wound care for patients with complicated wounds. In addition, Butter et al. [11] reported the early improvement of surgical wound dehiscence using NPWT in seven pediatric patients. NPWT was also effective for early wound healing in six patients with wound dehiscence caused by severe SSI in the present series. In particular, two patients had severe wound dehiscence caused by a large amount of local fluid from a small fistula connected to the gastrointestinal tract. The NPWT successfully closed the fistula and the wound dehiscence. These results and those of the previous studies indicate that NPWT provides excellent treatment for pediatric patients with wound dehiscence caused by SSI.

The ARS was administered to the patients with wound dehiscence caused by SSI in addition to treatment with NPWT. Arginine is a dietary, conditionally essential amino acid. About 50% of the ingested arginine is released into the portal circulation and the remaining arginine is then directly used in the small intestine [16,21]. The venous circulating arginine serves as the substrate for protein and collagen metabolism in extrahepatic tissues [16,21]. The kidney metabolizes citrulline, which is the major precursor for arginine, into arginine and exports arginine into the systemic circulation. Arginine possesses numerous
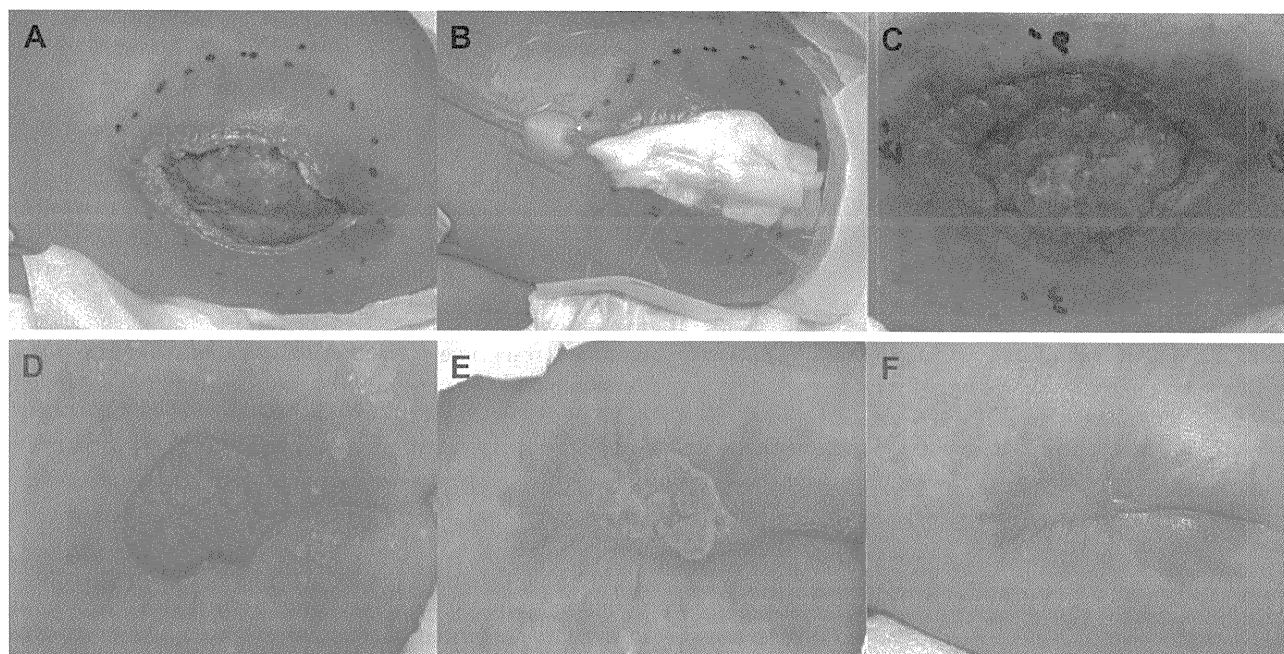
Fig. 1. Chronological change in wound dehiscence in patient number 2. (A) Wound appearance on the day of the wound dehiscence (postoperative day 12). (B) Negative pressure wound therapy (postoperative day 12). Wound appearance on the (C) 10th day after starting arginine-rich supplementation (postoperative day 32), (D) 20th day after starting arginine-rich supplementation (postoperative day 42), (E) 28th day after starting arginine-rich supplementation (postoperative day 50), and (F) 50th day after starting arginine-rich supplementation (postoperative day 72).

unique and potentially useful pharmacologic effects involving protein synthesis, the function of T-lymphocytes, and a positive nitrogen balance [16,21]. In addition, arginine is a substrate for nitric oxide, which has a critical role in vascular dilatation [16, 21]. Therefore, the administration of arginine leads to the improvement of local circulation in the wound dehiscence site [16,21]. In fact, the presence of nitric oxide produced from arginine has been suggested to help the transition of a wound from the acute inflammatory phase to the proliferative phase of wound healing [18]. Furthermore, arginine is involved with the two major catabolic pathways associated with wound healing, including the production of nitric oxide, cell proliferation, and collagen through its metabolism to ornithine and other poly-amines [18,19]. Therefore, recent clinical and experimental studies of arginine have focused on wound healing [13–20]. The administration of L-arginine leads to the restoration of decreased hydroxyproline levels, which is a metabolite of collagen synthesis, in the wound fluid, preventing a decrease in collagen I synthesis and increasing the wound breaking strength after traumatic hemorrhage [13,14]. In addition, the benefits of L-arginine administration on early wound healing have been clinically reported in patients with pressure ulcers and traumatic wounds [15–19]. However, there have been no reports of L-arginine enteral administration for the improvement of wound dehiscence caused by SSI. Therefore, ARS including L-arginine was administered to pediatric patients with wound dehiscence caused by SSI in addition to the introduction of NPWT. In fact, complete closure of the wound was recognized in patients with large complicated wound dehiscence an average of 3 wk after the introduction of combination therapy. The precise advantages of the individual therapies could not be shown in this study because it was not a comparison between this combination therapy and the traditional wound care therapy or only NPWT. However, the duration of this combination therapy for closure of

wounds was thought to be shorter than in other clinical reports describing only NPWT in pediatric surgical patients [8–12].

We used this combination therapy in patients with SSI without an acute inflammatory phase or a severe systemic inflammation. In a recent study, a special diet that included arginine failed to shorten a prolonged inflammatory phase and impaired healing in malnourished rats [22]. The results of this study indicate that previous undernutrition increases the inflammatory reaction after subsequent wounding and that this reaction almost certainly negatively modulates the process of wound healing [23]. It is likely that special diets enriched in arginine and trace elements do not have a positive effect, which is related to an increased production of nitrous oxide, in a severe inflammatory condition. Therefore, clinicians should avoid using ARS in patients with SSI in an acute inflammatory phase or a severe systemic inflammation.

In conclusion, this study demonstrated that the administration of ARS in addition to NPWT is effective for the improvement of wound dehiscence caused by SSI in infant patients after surgery. However, the number of patients investigated in this study was very small. Further studies in a larger group of infant patients will therefore be necessary to elucidate the usefulness of this combination therapy for wound dehiscence caused by SSI.

Acknowledgments

References

[1] Mangram AJ, Horan TC, Pearson ML, Silver LC, Jarvis WR. Hospital infection control practice advisory committee: guideline for prevention of surgical site infection. Infect Control Hosp Epidemiol 1999;20:247–78.

[2] Horan TC, Gaynes RP, Martone WJ, Jarvis WR, Emori TG. CDC definitions of noscomial surgical site infections. Infect Control Hosp Epidemiol 1992;13:606–8.

[3] Owens CD, Stoessel K. Surgical site infections: epidemiology, microbiology and prevention. J Hosp Infect 2008;70:3–10.

[4] Upperman JS, Sheridan RL, Marshall J. Pediatric surgical site and soft tissue infections. Pediatr Crit Care Med 2005;6:S36–41.

[5] Argenta LC, Morykwas MJ. Vacuum-assisted closure: a new method for wound control and treatment. Clinical experience. Ann Plast Surg 1997;36:563–76.

[6] Heller L, Levin SL, Butler CE. Management of abdominal wound dehiscence using vacuum assisted closure in patients with compromised healing. Am J Surg 2006;191:165–72.

[7] Subramonia S, Pankhurst S, Rowlands BJ, Lobo DN. Vacuum-assisted closure of postoperative abdominal wounds: a prospective study. World J Surg 2009;33:931–7.

[8] Mooney JF, Argenta LC, Marks MW, Morykwas MJ, de Franzo AJ. Treatment of soft tissue defects in pediatric patients using the V.A.C. system. Clin Orthop 2000;376:26–31.

[9] Caniano DA, Ruth B, Teich S. Wound management with vacuum-assisted closure: experience in 51 pediatric patients. J Pediatr Surg 2005;40:128–32.

[10] Arca MJ, Somers KK, Derks TE, Goldin AB, Aiken JJ, Sato TT, et al. Use of vacuum-assisted closure: system in the management of complex wounds in the neonates. Pediatr Surg Int 2005;21:532–5.

[11] Butter A, Emran M, Al-Jazaeri A, Ouimet A. Vacuum-assisted closure for wound management in the pediatric population. J Pediatr Surg 2006;41:940–2.

[12] Hiramatsu T, Okamura Y, Komori S, Nishimura Y, Suzuki H, Takeuchi T. Vacuum-assisted closure for mediastinitis after pediatric cardiac surgery. Asian Cardiovasc Thorac Ann 2008;16:e45–6.

[13] Wittmann N, Prix N, Mayr S, Angele P, Wichmann MW, van den Engel NK, et al. L-arginine improves wound healing after trauma-hemorrhage by increasing collagen synthesis. J Trauma 2005;59:162–8.

[14] Shi HP, Wang SM, Zhang GX, Zhang YJ, Barbul A. Supplemental L-arginine enhances wound healing following trauma/hemorrhagic shock. Wound Rep Reg 2007;15:66–70.

[15] Desneves KJ, Todorovic BE, Cassar A, Crowe TC. Treatment with supplementary arginine, vitamin C and zinc in patients with pressure ulcer: a randomized controlled trial. Clin Nutr 2005;24:979–87.

[16] Curran JN, Winter DC, Bouchier-Haynes D. Biological fate and clinical implications of arginine metabolism in tissue healing. Wound Rep Reg 2006;14:376–86.

[17] Heyman H, van de Looverbosch DE, Meijer EP, Schols JM. Benefits of an oral nutritional supplement on pressure ulcer healing in long-term care residents. J Wound Care 2008;17:476–80.

[18] Schols JM, Heyman H, Meijer EP. Nutritional support in the treatment and prevention of pressure ulcers: an overview of studies with an arginine enriched oral nutritional supplement. J Tissue Viab 2009;18:72–9.

[19] van Anholt RD, Sobotka L, Meijer EP, Heyman H, Groen HW, Topinkova E, et al. Specific nutritional support accelerates pressure ulcer healing and reduces wound care intensity in non-malnourished patients. Nutrition 2010;26:867–72.

[20] Wild T, Rahbarnia A, Kellner M, Sobtka L. EberleinT. Basics in nutrition and wound healing. Nutrition 2010;26:862–6.

[21] Witte MB, Barbul A. Arginine physiology and its implication for wound healing. Wound Rep Reg 2003;11:419–23.

[22] Alves CC, Torrinhas RS, Giorgi R, Brentani MM, Logullo AF, Arias V, et al. Short-term specialized enteral diet fails to attenuate malnutrition impairment of experimental open wound acute healing. Nutrition 2010;26:873–9.

[23] Sobotka L. Healing of wounds and pressure ulcers. Nutrition 2010;26:856–7.

ELSEVIER

Correlation between the number of segmental chromosome aberrations and the age at diagnosis of diploid neuroblastomas without *MYCN* amplification

Ryota Souzaki [a,*], Tatsuro Tajiri [a], Risa Teshiba [a], Yoshiaki Kinoshita [a], Ryota Yosue [a], Kenichi Kohashi [b], Yoshinao Oda [b], Tomoaki Taguchi [a]

[a]Department of Pediatric Surgery, Graduate School of Medical Sciences, Kyushu University, Fukuoka 812-8582, Japan
[b]Department of Anatomic Pathology, Graduate School of Medical Sciences, Kyushu University, Fukuoka 812-8582, Japan

Abstract
Background: In neuroblastomas (NBs) without *MYCN* amplification, segmental chromosome aberrations SCAs such as 1p loss, 11q loss, and 17q gain have been suggested to be associated with the prognosis of the patients. We assessed the correlation between the number of SCAs and other biological factors in primary NBs samples.
Method: The status of SCAs in 54 primary NBs samples was analyzed using the single-nucleotide polymorphism (SNP) array (Human CMV370-Duo; Illumina, San Diego, CA). The status of *MYCN* amplification was determined by an SNP array and the fluorescence in situ hybridization method. The DNA ploidy was determined by flow cytometry.
Results: Nine of 54 samples showed *MYCN* amplification. All 9 samples with *MYCN* amplification and 20 of 45 samples without *MYCN* amplification showed diploidy/tetraploidy, and the other 25 samples without *MYCN* amplification showed aneuploidy. The most frequent SCAs were 17q gain (26/54; 48.1%) and 11q loss (16/54; 29.6%), followed by 1p loss (15/54; 27.8%). The number of SCAs in diploidy/tetraploidy NBs without *MYCN* amplification (7.00 ± 4.67) was higher than that in NBs with *MYCN* amplification (4.78 ± 2.82) and in aneuploid NBs (1.64 ± 2.78) ($P < .05$). In diploid/tetraploid NBs without *MYCN* amplification, there was a significant difference between an age at diagnosis less than 12 months (n = 7) and over 12 months (n = 13) (4.14 ± 3.63 vs 8.54 ± 4.54; $P = .04$). Moreover, the number of SCAs correlated with the age at diagnosis in diploid/tetraploid samples without *MYCN* amplification ($r = 0.70$, $P = .0006$). In NBs with *MYCN* amplification, the number of SCAs did not correlate with the age at diagnosis.
Conclusion: The number of SCAs significantly increased in proportion to age at diagnosis in diploid/tetraploid NBs without *MYCN* amplification. The increase in the number of these SCAs may play an important role in the prognosis of patients without *MYCN* amplification over 12 months of age.
© 2011 Elsevier Inc. All rights reserved.

Neuroblastoma (NBs) is the most common extracranial solid malignant tumor in children. It originates from the sympathetic nervous system and usually occurs in the

adrenal medulla. Despite the increasing knowledge about the biology of NBs, the survival rate of high-risk NBs patients is still poor [1].

Several genetic markers of NBs have been shown to provide prognostic information. For example, with regard to the ploidy of NBs, in contrast to diploidy/tetraploid NBs, triploid tumors are associated with a good outcome [2]. *MYCN* gene amplification occurs in approximately 25% of primary NBs, and NBs with *MYCN* amplification show a poor prognosis [3-5]. In NBs without *MYCN* gene amplification, genetic instability as the segmental chromosome aberration (SCAs), such as a 1p loss, 3p loss, 11q loss, and 17q gain [6,7], is another poor prognostic factor. However, in NB samples, SCAs are found in not only 1p, 3p, 11q, and 17q but also in other chromosomes. The correlation between the number of SCAs and the prognosis of NBs is not revealed.

Genome-wide high-resolution screening methods, such as single-nucleotide polymorphism (SNP) [8,9], comparative genomic hybridization (CGH) [10], and other arrays have recently been used to detect the biological alterations in NBs samples instead of low-resolution approaches such as G-banded chromosome analysis. These genome-wide analyses have facilitated and accelerated the known copy number alterations of NBs.

In the present study, we determined the SCAs in 54 NBs patients using a high-resolution SNP array to analyze their association the number of SCAs with other prognostic markers of NBs, such as *MYCN* amplification, age at diagnosis and ploidy.

1. Materials and methods

1.1. Patient clinical data and biological data of NB samples

Patients with NB, evaluated in the Department of Pediatric Surgery in Kyushu University, were diagnosed between April 1988 and March 2008. The tumors were staged according to the International Neuroblastoma Staging System (INSS). All of the parents of the patients provided their informed consent for tumor preservation and the biological analysis before surgery. We have obtained the comprehensive agreement for all samples. This study was performed according to ethical guidelines for clinical studies of the Ministry of Health, Labour and Welfare of Japan. Fifty-four NBs samples were obtained from untreated patients. The patient clinical data and biological data of all NB samples are shown in Table 1. The patients included 30 boys and 24 girls; 12 were stage 1 according to the INSS, 4 were stage 2, 8 were stage 3, 26 were stage 4, and 4 were stage 4S. Thirty had been diagnosed when they were younger than 12 months of age (median 12 months old, 0-108 months). Nine patients were identified by a mass screening system in Japan at 6 months old. DNA ploidy was

Table 1   Patient clinical and biological data of NB samples

Clinical data	
Sex	
Male	30
Female	24
Age	
<12 mo	30
≥12 mo	24
Mass screening	
Positive	9
Negative	45
INSS	
1	12
2	4
3	8
4	26
4S	4
Biological data	
Ploidy	
Diploid/tetraploid	29
Aneuploid	25
MYCN amplification (+)	9
MYCN amplification (−)	45

determined by flow cytometry in all 54 specimens [11], and *MYCN* amplification was determined by fluorescence in situ hybridization (FISH) and SNP array. All 54 samples were grouped by three groups based on the difference of the tumor biology. The diploid/tetraploid samples with *MYCN* amplification are identified as group 1. The diploid/tetraploid samples without *MYCN* amplification are identified as group 2. The aneuploid samples without *MYCN* amplification are identified as group 3.

1.2. SNP array

DNA was extracted from tumor samples and purified using the standard method. The DNA was subjected to an SNP array analysis using Human CMV370-Duo (Illumina, San Diego, CA) according to the manufacturer's protocol. Genomic profiles were created using the Illumina Genome Viewer and Chromosome Browser of Illumina's BeadStudio3.0 software program. All samples showed call rates greater than 0.99. We counted the number of SCAs in each chromosome for all samples.

1.3. FISH method

The gene dosage of the *MYCN* gene was determined by a FISH analysis as described previously [12]. The *MYCN* gene probe (LSI N-MYC SO; Vysis) or *MYCN* gene and the α satellite region of human chromosome 2 probes (LSI N-MYC SG/CEP 2 SO DNA probe; Vysis) were used. The signals representing the *MYCN* gene and the centromeric region of chromosome 2 were counted in 100 cells on each slide. The *MYCN* amplification was defined as an increase of

Table 2   SCAs and *MYCN* gene amplifications

	Group 1 (n = 9)	Group 2 (n = 20)	Group 3 (n = 25)	Total (n = 54)
17q gain	8/9 (88.9%)	13/20 (65.0%)	5/25 (16.0%)	26/54 (48.1%)
11q loss	3/9 (33.3%)	11/20 (55.0%)	2/25 (8.0%)	16/54 (29.6%)
1p loss	9/9 (100%)	5/20 (25.0%)	1/25 (4%)	15/54 (27.8%)
2p gain	2/9 (22.2%)	7/20 (45%)	2/25 (8%)	11/54 (20.4%)
3p loss	1/9 (11.1%)	9/20 (45%)	1/25 (4%)	11/54 (20.4%)

over 4-fold of *MYCN* signals in relation to the number of chromosome 2 signals in a dual-color probe or over 8 *MYCN* signals in a single-color probe.

1.4. Statistical analyses

Data were analyzed using Student t test. The results are expressed as the means ± SD for the number of SCAs of NBs samples. We determined Pearson correlation co-efficients between the number of SCA and the age at diagnosis. The χ^2 test was used for statistical analysis. We calculated the *P* values, with *P* < .05 set to indicate statistical significance.

2. Results

2.1. SCAs and *MYCN* gene amplifications

Nine of 54 samples showed *MYCN* amplification. All 9 samples with *MYCN* amplification (group 1) and 20 of 45 samples without *MYCN* amplification showed diploidy/tetraploidy (group 2), and other 25 samples without *MYCN* amplification showed aneuploidy (group 3). One or more SCAs were detected in 37 (68.5%) of all 54 samples. In all 54

samples, the most frequently observed SCAs were 17q gain (26/54; 48.1%) and 11q loss (16/54; 29.6%), followed by 1p loss (15/54; 27.8%) (Table 2). The 1p loss and 17q gain occurred frequently in NBs samples with group 1, whereas the 11q loss, 2p gain, and 3p loss occurred more frequently in NBs samples with group 2.

Fig. 1 showed the number of SCAs in three groups. The number of SCAs in group 2 (7.00 ± 4.67) was significantly higher than that in group 1 (4.78 ± 2.82) and group 3 (1.64 ± 2.78) (*P* < .05).

2.2. Correlation between the number of SCAs and the age at diagnosis

There was a significant difference between the age at diagnosis (<12 months, n = 7, and >12 months, n = 13; 4.14 ± 3.63 vs 8.54 ± 4.54, *P* = .04) in group 2. Fig. 2 shows that there was a significant (*r* = 0.70, *P* = .0006) correlation between the number of SCAs and the age at diagnosis in group 2. All 7 patients that died due to the tumor showed 8 or more SGAs. In group 2, the number of SCAs in the patients that died (n = 7) was significantly higher than that in the survivors (n = 13) (9.86 ± 2.48 vs 5.46 ± 4.91, *P* = .04).

On the other hand, in samples with group 1, the number of SCAs did not correlate with the age at diagnosis (*r* = 0.13, *P* = .726) (Fig. 3), and there was not significantly difference between the number of SCAs in
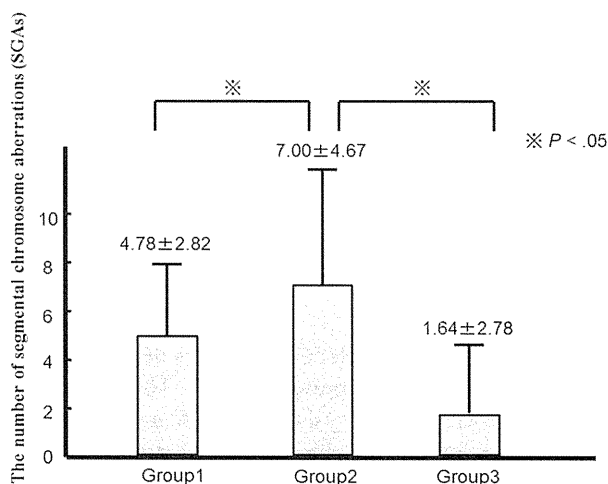

Fig. 1   The number of SCAs in 3 groups. The number of SCAs in group 2 (7.00 ± 4.67) was higher than that in group 1 (4.78 ± 2.82) and group 3 (1.64 ± 2.78) (*P* < .05).
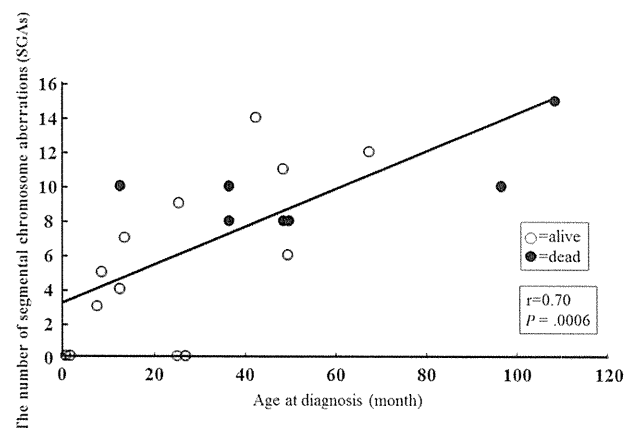

Fig. 2   The correlation between the number of segmental aberrations and the age at diagnosis in samples without *MYCN* amplification (*r* = 0.70, *P* = .0006).
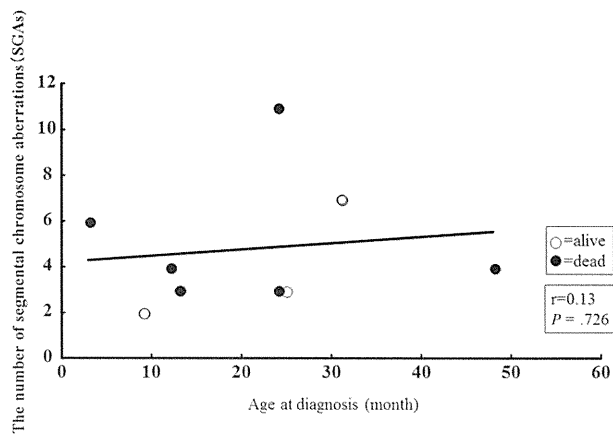
Fig. 3 The correlation between the number of segmental aberrations and the age at diagnosis in samples with *MYCN* amplification ($r = 0.13$, $P = .726$).

the patients that died (n = 6; 5.16 ± 3.06) and that in the survivors (n = 3; 4.00 ± 2.65).

3. Discussion

In the present study, the number of SCAs such as 11q loss, 17q gain, and 1p loss, significantly increased in proportion to the age at diagnosis in patients with diploid/tetraploid NBs without *MYCN* amplification. Spitz et al [13] previously reported that 11q and 3p loss were also associated with advanced stage disease and that the children with 11q deletion and 3p deletion were older than those with normal 11q and normal 3q loss. 17q gain was reported to be associated with factors related to a poor prognosis, such as advanced stage disease, *MYCN* amplification, age at diagnosis, and ploidy [14]. These SCAs therefore affect the patient prognosis. However, in NBs samples, segmental chromosomal gain and loss are found in not only 1p, 3p, 11q, and 17q but also in other chromosomes [15]. This is the first report on the association between the number of SCAs with the age at diagnosis and the prognosis in diploid/tetraploid NBs without *MYCN* amplification.

The number of SCAs in aneuploid samples is low in the current study. In aneuploid tumors, whole chromosomal gain and loss were more common. Therefore, there is no significant correlation between the number of SCAs and the age at diagnosis and the prognosis (data are not shown). However, only 1 patient with aneuploidy died due to the tumor in the current study. This case had 3 SCAs (9p gain, 11q loss, and 17q gain). The 11q loss and 17q gain are poor prognostic factors in diploid tumors, and therefore, these SCAs may have been responsible for the poor prognosis of this patient.

Our study also showed that the number of SCAs increases as the age at diagnosis increases for subjects with diploid

NBs. Diploid NBs may be unstable; therefore, segmental gains and losses may accumulate over time in the presence of diploidy. When NBs develop poor prognostic abnormalities such as 11q, 3p loss, and 17q gain, there may be an increase in the speed of tumor growth, which leads to the onset of symptoms. On the other hand, in samples with *MYCN* amplification, the number of SCAs did not correlate with the age at diagnosis in our study. In our study, *MYCN* amplified patients are 9. Therefore, a larger number of cases must therefore be studied to elucidate this point.

In conclusion, the number of SCAs significantly increases in proportion to the age at diagnosis in subjects with diploid/tetraploid NBs without *MYCN* amplification. The increase of the number of these SCAs may play an important role in the prognosis of the patients without *MYCN* amplification.

References

[1] Cotterill SJ, Pearson AD, Pritchard J, et al. Clinical prognostic factors in 1277 patients with neuroblastoma: results of The European Neuroblastoma Study Group 'Survey' 1982-1992. Eur J Cancer 2000;36:901-8.

[2] Look AT, Hayes FA, Nitschke R, et al. Cellular DNA content as a predictor of response to chemotherapy in infants with unresectable neuroblastoma. N Engl J Med 1984;311:231-5.

[3] Brodeur GM, Maris JM, Yamashiro DJ, et al. Biology and genetics of human neuroblastomas. J Pediatr Hematol Oncol 1997;19:93-101.

[4] Brodeur GM, Seeger RC, Schwab M, et al. Amplification of N-myc in untreated human neuroblastoma correlates with advanced disease stage. Science 1984;224:1121-4.

[5] Seeger RC, Brodeur GM, Sather H, et al. Association of multiple copies of the Nmyc oncogene with rapid progression of neuroblastomas. N Engl J Med 1985;313:1111-6.

[6] Guo C, White PS, Weiss MJ, et al. Allelic deletion at 11q23 is common in MYCN single copy neuroblastomas. Oncogene 1999;18: 4948-57.

[7] Plantaz D, Mohapatra G, Matthay KK, et al. Gain of chromosome 17 is the most frequent abnormality detected in neuroblastoma by comparative genomic hybridization. Am J Pathol 1997;150:81-9.

[8] Tajiri T, Souzaki R, Kinoshita Y, et al. Risks and benefits of ending of mass screening for neuroblastoma at 6 months of age in Japan. J Pediatr Surg 2009;44:2253-7.

[9] Souzaki R, Tajiri T, Teshiba R, et al. The genetic and clinical significance of MYCN gain as detected by FISH in neuroblastoma. Pediatr Surg Int 2011;27:231-6.

[10] Spitz R, Oberthuer A, Zapatka M, et al. Oligonucleotide array-based comparative genomic hybridization (aCGH) of 90 neuroblastomas reveals aberration patterns closely associated with relapse pattern and outcome. Genes Chromosomes Cancer 2006;45:1130-42.

[11] Taylor SR, Roedere M, Murphy RF. Flow cytometric DNA analysis of adenocortical tumors in children. Cancer 1987;59:2059-63.

[12] Souzaki R, Tajiri T, Higashi M, et al. Clinical implications of a slight increase in the gene dosage of MYCN in neuroblastoma determined using quantitative PCR. Pediatr Surg Int 2008;24:1095-100.

[13] Spitz R, Hero B, Ernestus K, et al. Deletions in chromosome arms 3p and 11q are new prognostic markers in localized and 4s neuroblastoma. Clin Cancer Res 2003;9:52-8.

[14] Bown N, Cotterill S, Lastowska M, et al. Gain of chromosome arm 17q and adverse outcome in patients with neuroblastoma. N Engl J Med 1999;340:1954-61.

[15] George RE, Attiyeh EF, Li S, et al. Genome-wide analysis of neuroblastomas using high-density single nucleotide polymorphism arrays. PLoS One 2007;28(2):e255.

Significance of Abnormalities in Systems Proximal and Distal to the Obstructed Site of Duodenal Atresia

Fatima S. Alatas, Kouji Masumoto, Genshiro Esumi, Kouji Nagata, and Tomoaki Taguchi

ABSTRACT

Background: Duodenal atresia (DA) is a well-known neonatal intestinal disease. Even after surgery, the proximal segment can continue to be severely dilated with hypoperistalsis, resulting in intestinal dysmotility problems in later life. No data have been published regarding the morphologic differences between the proximal and distal regions of obstructed sites of the intramural components in DA.
Methods: Operative duodenal samples (N = 12) from cases with DA (age 1–3 days) were used. Age-matched controls (N = 2) were used. All of the specimens were immunohistochemically stained with antibodies to S-100 protein, α-smooth muscle actin, and c-kit protein.
Results: At the proximal segments of the obstructed site in DA, the number of neuronal cells decreased in size and number. The circular musculature was moderately to severely hypertrophic. Unusual ectopic smooth muscle bundles were also identified. The innermost layer of the circular musculature was thinner. Interstitial cells of Cajal are decreased, even around the myenteric plexus. All of the staining in the distal segments in DA was similar to the control tissues.
Conclusions: Proximal and distal segments in DA differ in the neural cells, musculature, and distributions of the interstitial cells of Cajal. Based on the present study, these morphologic changes may contribute to the onset of postoperative duodenal dysmotility.

Key Words: α-smooth muscle actin, duodenal atresia, interstitial cells of Cajal, neural cells

(JPGN 2012;54: 242–247)

D uodenal atresia (DA) is a well-known intestinal disease, which frequently causes intestinal obstruction in newborns, and it is commonly associated with other congenital anomalies (1,2). DA accounts for 25% to 40% of all cases with intestinal atresia (IA) (3). The frequency of DA in Japan is reported to be 1 in 3000 to 5000 live births.

Various surgical procedures to anastomose the proximal dilated site to the distal site, such as duodenoduodenostomy and duodenojejunostomy, have been introduced with promising results (4–7). Successful surgical repair has also been reported, with a mortality rate as low as 3% to 5% after correction, in addition to an excellent long-term survival rate (8–10). Even after successful surgery, however, the proximal site can continue to be severely dilated with hypoperistalsis, resulting in intestinal dysmotility problems in later life (11). Dysmotility problems in DA appear to be caused by a dilatation of the intestine proximal to the obstructed site, which has not been adequately resected. Intestinal dysmotility often leads to functional obstruction characterized by marked dilatation resulting from ineffective peristalsis (12–14). These findings have been supported by previous manometric studies, which found a reduction in the intraluminal manometric pressure and a transit disturbance in the dilated proximal intestines (15,16).

Similar to other types of IA, in DA, hyperplasia and hypertrophy of the smooth muscle are found in varying degrees in the proximal site of obstruction, whereas these same conditions are rarely observed at the distal site of the obstruction (17,18). Chick studies have demonstrated several abnormalities in the intramural nervous system, muscular elements, and the interstitial cells of Cajal (ICC) in the proximal dilated segment of the IA. These findings were found not only in human samples of patients with IA but also in a chick IA model (11,19). There are no published data describing the differences between the proximal and distal sections of obstructed sites regarding the intramural components in patients with DA. In the present study, we investigated the morphologic differences in the enteric nervous system, the ICC, and smooth muscle, between the regions proximal and distal to the obstructed site in neonates with DA, to enhance our understanding of motility problems in patients with DA.

METHODS

Tissue Specimens

Twelve resected duodenal samples obtained from neonates with DA who were delivered at Kyushu University Hospital (Fukuoka, Japan) were used in the present study after obtaining the approval of the university ethics committee. The subjects' gestational ages were 34 to 40 weeks, and the duodenal samples were obtained at the primary operation during the subjects' first to third days after birth. The 0.5-cm anterior walls of both the proximal and distal segments apart from the obstructed site were collected as samples. Age-matched duodenal samples of controls were obtained from 2 patients without gastrointestinal disease at an autopsy (congenital diaphragmatic hernia). The number of control material samples was insufficient because of the difficulty in obtaining normal controls for the present study. Formalin-fixed, paraffin-embedded tissues were cut into 4-μm-thick slices and were processed for immunohistochemistry.

Immunohistochemistry

Duodenal specimen slices were stained with hematoxylin and eosin to evaluate the presence of the submucosal and myenteric

plexus and the smooth muscle layer before performing immuno-histochemical staining.

All of the specimens were immunohistochemically stained using the standard avidin-biotin complex method. The primary antibodies were a polyclonal antibody to S-100 protein (code no. 422091 Nichirei Co Ltd, Tokyo, Japan) as a general neuronal marker and an antibody to c-kit protein (CD-117, diluted 1:100; DakoCytomation, Carpinteria, CA) as a marker of ICC, and a monoclonal antibody to α-smooth muscle actin (α-SMA, clone IA4, diluted 1:200; Sigma Immunochemicals, St Louis, MO) as a general muscle marker (Table 1).

In brief, after deparaffinization in xylene and dehydration in 100% alcohol, slides were treated with 3% H_2O_2 in methanol to block endogenous peroxidase activity. For antigen retrieval, the slides were subjected to 10 minutes of microwave treatment in citric acid buffer (pH 6.0). After cooling to room temperature, the slides were incubated with an undiluted blocking solution (Histofine, SAB-PO [MULTI] Kit; Nichirei) containing goat serum albumin. After rinsing with phosphate-buffered saline (PBS), the slides were incubated with a primary antibody (Table 1). The slides were rinsed twice with PBS and incubated for 10 minutes with an undiluted biotinylated secondary antibody (Histofine). Slides were then rinsed again twice with PBS followed by incubation for 10 minutes with undiluted peroxidase-conjugated streptavidin (Histofine). In all of the duodenal specimens stained, peroxidase was detected by dia-minobenzidine tetrahydrochloride (Histofine, DAB Kit, Nichirei) with purified water for 5 minutes. Finally, the slides were rinsed with running tap water and counterstained with hematoxylin, dehydrated through a graded alcohol series, and washed with xylene.

Evaluation and Analysis

The morphologic differences were evaluated among the proximal and distal segments of the obstructed sites of DA samples and compared with those of the controls. In addition, the differences between the segments were quantitatively presented. For quantitative evaluation, all of the sections were photographed using light microscopy using 4×, 10×, 20×, and 40× magnifications. The quantification of the immunoreactivities of c-kit were evaluated from each slide by measuring the length of the c-kit-positive area, and the immunoreactivities of S-100 were evaluated from each slice by measuring the length of each stained ganglion or plexus. The α-SMA antibody immunoreactivities were quantified by measuring the thickness of the longitudinal muscle layer, the circular muscle layer, and the muscularis mucosae in 3 different locations. The mean values of the 3 area measurements are presented in Results. All of the measurements were taken using the ImageJ version 1.43s software program (National Institutes of Health, Bethesda, MD) in an area 4080 × 3072 pixels wide, and then were converted to micrometers according to each magnification. The differences

between the c-kit-positive area, the length of the neuronal cells, and the width of the mucosal muscle layers of the proximal and distal segments were compared using the Student t test. Differences between the width of the circular muscle layer and the longitudinal muscle layer of the proximal and distal segments were compared using the Mann-Whitney U test. $P < 0.05$ were considered to be statistically significant. All of the statistical analyses were performed with the SPSS statistical software program (SPSS Inc, Chicago, IL).

RESULTS

The present study included 9 patients with type III and 3 patients with type I DA. All of the patients had been antenatally diagnosed as having DA during the prenatal period; therefore, all of the patients were treated in our department after the immediate diagnosis for the confirmation of DA following birth. In all of the patients, a longitudinal incision and a transverse duodenoduode-nostomy (diamond-shape anastomosis) or membranous resection was performed 1 to 3 days after birth.

S-100 Protein Staining

In the control samples, immunoreactivity to S-100 antibody was observed in the myenteric, submucosal plexuses, and nerve fibers distributed throughout the entire bowel wall layers. Auerbach plexus between the circular and longitudinal muscle layers was clearly labeled by S-100 protein immunostaining. Several positive fibers were also detected in the muscularis mucosae and in the villus of the lamina propria (data not shown). In the proximal segment of the obstructed sites in the cases with DA, an abnormal nervous distribution showing S-100-positive immunoreactivity was observed (Fig. 1A, B). In the myenteric plexus, the number and size of the S-100-positive plexus were smaller than those in the distal segments and the controls. In addition, a small number of ganglion cells were also observed. The ganglion cells were small and immature compared with those of the distal segments and the controls. Nerve fibers observed between the circular and the longitudinal musculature not only were fewer in number but also were composed of smaller fibers. The size and length of the ganglionic cells were also smaller than those of the distal segments and the controls, especially in the area where hypertrophic muscu-lature was observed (Fig. 1A, B). In contrast, the nervous distri-bution of the distal segment of obstructed site was undistinguishable from those of controls (Fig. 1C, D). Quantitative analyses showed a significantly shorter ganglion length and plexus of the proximal segments than was observed in the distal segments of the obstructed site (proximal $203.43 \pm 103.49 \mu m$, distal $297.67 \pm 136.58 \mu m$, $P = 0.002$, Table 2). There was no significant difference in the length of the ganglion and myenteric plexus between the distal segments of the obstructed site and control tissues ($P = 0.134$).

TABLE 1. Antibodies used to evaluate the nervous system, ICC, and smooth muscle layers

Antibody	Code no./clone no.	Species	Dilution	Manufacturer	Marker
S-100	422091	Rabbit polyclonal	5 $\mu g/mL$	Nichirei Co Ltd, Tokyo, Japan	Ganglion cells and nerve fiber
α-Smooth muscle actin	1A4	Mouse monoclonal	1:200	Sigma Immunochemicals, St Louis, MO	Smooth muscle cells
c-kit	CD-117	Rabbit polyclonal	1:100	DakoCytomation, Carpinteria, CA	ICC

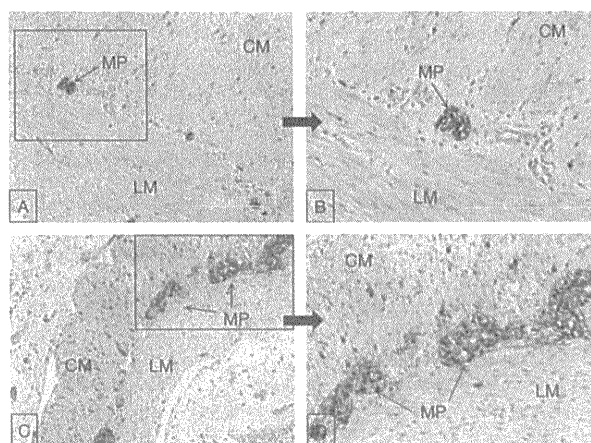ICC = interstitial cells of Cajal.

— 124 —

FIGURE 1. The duodenum shows the distribution of S-100 immunoreactive nerve cells and nerve fibers (original magnification 10×, 20×). A, B, The proximal segment of obstructed site of patients with duodenal atresia. The myenteric plexus (MP) was markedly reduced in size and distribution and also contained hypoplastic cells. C, D, The segment distal to the obstructed site in a sample of patients with duodenal atresia. The distribution pattern of the positive nerve cell end fibers is nearly identical to the control samples. CM = circular musculature; LM = longitudinal musculature.

α-SMA Staining

In the control samples, a homogenous immunoreactivity to the α-SMA antibody was observed in all of the muscle layers: the muscularis mucosae, circular muscle layer, and the longitudinal muscle layers (data not shown). In the proximal segment of the obstructed site in samples of patients with DA, a moderately to severely hypertrophic area was observed in the circular and longitudinal muscle layers, particularly in the circular muscle layers, compared with those of the distal segments or the controls (Fig. 2A, B, C). The innermost layer of the circular muscle layer in the proximal segments was also thinner and was nearly undetectable in some sections, compared with those in the distal segments or the controls. In addition, in all of the patients, unusual ectopic muscle bundles were found around the submucosal connective tissue near the innermost layer of the circular muscle layers (Fig. 2B). These smooth muscle bundles originated from the muscle bundle in the

thin innermost circular muscle layer. In addition, the muscularis mucosae were also found to be hypertrophic (Fig. 2C). In contrast, in the distal segments of the obstructed site in DA, the staining pattern of α-SMA antibody was similar to that observed in the control samples (Fig. 2D, E, F). There was no significant difference in quantitative analyses of the thickness of the circular muscle layers, the longitudinal muscle layers, and the muscularis mucosae between the distal segments of obstructed sites and control tissues ($P = 0.646$, $P = 598$, and $P = 0.395$, respectively). In contrast, quantitative analyses revealed a significant difference in the thickness of the muscularis mucosae of the proximal segments compared with the distal segments of the obstructed site (proximal $36.46 \pm 13.51 \, \mu m$, distal $12.52 \pm 6.06 \, \mu m$, $P < 0.001$, Table 2). Quantitative analyses also revealed a significant difference between the circular muscle layers of the proximal and distal segments of the obstructed site (proximal $492.91 \, \mu m$ [range $263.19–733.16 \, \mu m$], distal $164.94 \, \mu m$ [range $135.61–199.37 \, \mu m$], $P < 0.001$, Table 2). There was also a significant difference between the proximal and distal segments of the longitudinal muscle layers (proximal $317.64 \, \mu m$ [range $110.73–369.18 \, \mu m$], distal $96.28 \, \mu m$ [range $73.83–121.20 \, \mu m$], $P < 0.001$, Table 2).

C-kit Staining

In the control samples, c-kit-positive cells were observed between the intermuscular space of the circular and longitudinal muscle layers, particularly around Auerbach plexus (data not shown). A small number of positive cells also were localized to the circular and longitudinal muscle layers and in the innermost layer of the circular muscle layers. In the proximal segment, the number of c-kit-positive cells was markedly decreased (Fig. 3A, B). Moreover, in some samples, the ICC were barely detectable, even around the myenteric plexus. The positive cells were bipolar in shape. Macrophage-like cells positive for c-kit staining were also observed within the muscularis propria and the submucosal area. Unlike the proximal segments, the distribution pattern and c-kit immunoreactivity in the ICC of the segment distal to the obstructed site were similar to those of the control samples (Fig. 3C, D; $P = 0.133$). These cells formed a network with cell-cell contacts and their shape was multipolar. The quantitative analyses revealed a significantly smaller c-kit-positive area in the proximal segments compared with the distal segments of the obstructed site (proximal $933.45 \, \mu m^2/mm^2$ [range $297.87–3149.62 \, \mu m^2/mm^2$], distal $12006.42 \, \mu m^2/mm^2$ [range $2473.79–22458.1 \, \mu m^2/mm^2$], $P < 0.001$, Table 2).

DISCUSSION

As a part of the normal growth process in the embryo from the fourth to the seventh week of gestation (embryo length 8.6–14.5 mm), the epithelial cells of the duodenum begin to proliferate

TABLE 2. Imunoreactivity comparison of the c-kit protein, S-100 protein, and α-smooth muscle actin antibody staining in the proximal and distal segments of obstructed site in samples of patients with duodenal atresia

	Proximal to obstructed site	Distal to obstructed site	P	Normal control
Nervous system (length/field)	203.43 μm (103.49)	297.67 μm (136.58)	0.002	373.27 μm (143.09)
Circular muscles layers thickness	492.91 μm (263.19–733.16)	164.94 μm (135.61–199.37)	<0.001	158.91 μm (34.07)
Longitudinal muscle layers thickness	317.64 μm (110.73–369.18)	96.28 μm (73.83–121.20)	<0.001	106.54 μm (13.34)
Muscularis mucosae thickness	36.46 μm (13.51)	12.52 μm (6.06)	<0.001	14.92 μm (2.89)
ICC positive area, μm²/mm²	933.45 μm²/mm² (297.87–3149.62)	12,006.42 μm²/mm² (2473.79–22,458.1)	<0.001	20,717.36 μm²/mm² (5925.64)

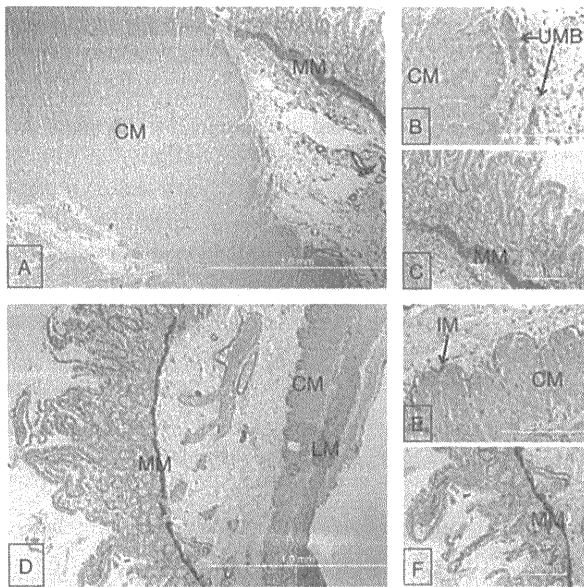Data are presented as mean (SD); median (25%–75%). ICC = interstitial cells of Cajal; SD = standard deviation.

FIGURE 2. The duodenum shows the distribution of immunoreactivity to α-smooth muscle actin antibody (original magnification 4× and 20×). A, B, C, The segment proximal to the obstructed site in a sample of patients with duodenal atresia. The circular musculature (CM) is moderately to severely hypertrophic. Unusual muscle bundles (UMB) with an oblique configuration were observed in the submucosal area, and the muscularis mucosae (MM) were hypertrophic. D, E, F, The distal segment of the obstructed site in a sample of patients with duodenal atresia. The lamina propria, the MM, the innermost layer of circular musculature (IM), and the longitudinal musculature (LM) are immunolabeled for α-smooth muscle actin antibody and are similar to those of the controls.

FIGURE 3. The duodenum showed the distribution of immunoreactivity to c-kit antibody (original magnification 10× and 20×). A, B, The proximal segment of the obstructed site in a sample of patients with duodenal atresia. There were few or no positive cells around the myenteric plexus (MP). C, D, The distal segment of the obstructed site in a sample of patients with duodenal atresia. Numerous positive cells were located around the MP, and a few positive cells were also distributed in the intermuscular space of the circular musculature (CM). LM = longitudinal musculature; ICC = interstitial cells of Cajal.

and completely plug the lumen (solid phase). Therefore, between the 15- and 65-mm stages (from the end of the 7th week to the 12th week of gestation), a process of vacuolization, coalescence of vacuoles, and recanalization occurs. DAs, stenosis, and intraluminal webs are believed to be caused by insults resulting in recanalization failure during the lengthening and rotation of the primitive foregut. A resultant obstruction is then believed to cause the dilatation in the proximal duodenum (20–22).

Using histochemical techniques, we have herein provided the first study of the potential differences in abnormalities of the smooth muscle, nervous system, and ICC between the segments proximal and distal to the obstructed site in samples from patients with DA. These 3 enteric components, which are involved in peristaltic activity, were immunohistochemically analyzed.

Although the etiology of DA is not the same as that in other IAs, the morphologic changes of the intestine in DA are thought to be similar. The morphologic change of the proximal segment seems to depend on the postobstructive dilatation during the fetal period. Similarly, in other forms of IA, morphologic change in the proximal segments also depends on the change after the formation of the obstruction.

In an experimental model of IA, several studies showed that the dilatation of the proximal segment induces the involution and lysis of the ganglion cells after initial hyperplasia of the myenteric
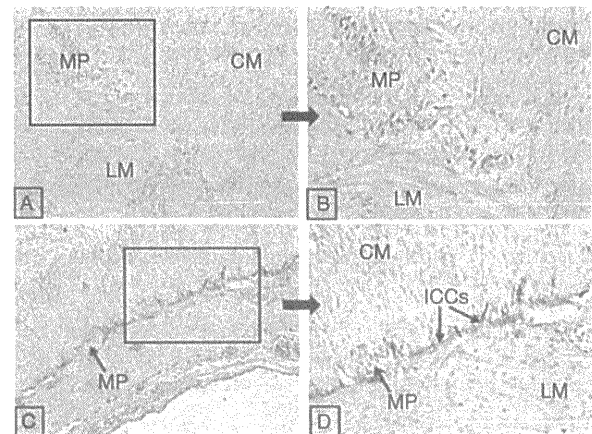
ganglia has occurred and irreversible distension continues to develop (23). Another possible cause of nerve alteration could be ischemic influence during fetal life through vascular disruption as shown in IA models (19,23). In the present study, we observed that in the area in which muscular layers are severely dilated, the distribution of ganglion and plexus is also less than that of the area with moderately dilated muscular layers. This finding supported a previous IA study (19), which observed marked abnormal neuronal changes in the distended proximal segments. In contrast, the neuronal distribution in the distal segment was close to normal in these studies, as in our study of human DA. The influence of muscular distention on the neuronal cell alteration is also shown in our previous case report of IA (24). In this case report, an improvement in numbers of neuronal cells and fiber distribution between primary operation of IA at 2 days after birth and second operation for the reconstruction of the dilated proximal segment at 6 months of age was observed (24). These abnormalities are probably a result of the developmental delay in the nervous system or of the dilatation of the proximal segment in DA, as mentioned in IA studies, which also found an alteration of enteric nerves in a severely dilated area of the proximal segment (11).

When examining smooth muscle morphology in the present study, we observed that the muscle layers in the proximal segments of the obstructed site are moderately to severely hypertrophic, unlike in the distal segments, which are indistinguishable from those of the control samples. This muscular hypertrophy has been well documented and results from a compensatory process following obstruction during the prenatal period, and it is localized exclusively to the circular musculature of the distended proximal intestinal segment (23,25,26). As mentioned in the literature, dysmotility of the intestine is often encountered in a severely dilated muscle of the segment proximal to the obstructed site. To prevent recurrence of the dilated segment, the markedly dilated

duodenum must be completely reconstructed surgically. Even after reconstruction surgery, however, a proximal segment consisting of a hypertrophic area remains because of the difficulty in visualizing the healthy area and minimizing the resected segment. Previous investigators have shown that the contractile pressure in the dilated proximal intestine of an IA model is lower than that in normal intestines. Moreover, physiologic studies of humans and animal models of IA have also shown a decrease in the motor activity in both the proximal and distal segments. These studies suggest that low contractile pressure was involved in the postoperative dysmotility (17). In addition, the existence of unusual muscle bundles, which have an oblique configuration, likely contributes to the disturbed bowel rhythms. Similar findings have been described in our previous study of cases with IA (17). Therefore, the existence of both hypertrophy of the circular muscle layers and unusual muscle bundles in the submucosal layers likely contributes to the development of motility disorders later in life, even after a successful initial operation. Additional procedures, such as intestinal plication or tapering the dilated intestine, are sometimes needed to produce efficient peristalsis of the proximal intestines.

Of particular interest with regard to the occurrence of unusual muscle bundles, our previous study of human IA showed that the smooth muscle bundles which emerged from the innermost layer of the circular musculature could be of either an oblique or vertical orientation to the long axis of the intestines, stretching toward mucosae, forming a coarse, irregular meshwork in the submucosa (17). Based on the chronologic view of our previous study of myogenesis in chick embryos, it is supposed that these muscle bundles may be a remnant of early developmental stages during the formation of the muscularis mucosae (27). Another study also proposed that a possible explanation for this phenomenon is that the ectopic muscle bundles are a secondary reaction of muscle cells to the chronic and progressive dilatation of the proximal segments. Moreover, these bundles also could indicate a secondary regressive reaction, which the proliferating reaction of regressive smooth muscle cells undergo when they first emerge in the inner layer of the circular muscle layer; thereafter, these smooth muscle cells protrude from the inner layer of the circular muscle layer to the layer of muscularis mucosae, according to the rules of normal development. The real causality regarding the development of ectopic muscle bundles in the proximal segment of the DA remains unclear, and the proposed reasons are based mostly on experimental IA, which is probably not appropriate for DA because of differences in the underlying etiology (27,28).

The small intestine exhibits rhythmic and phasic contractions that form the basis for propagating and segmental contraction. These rhythmic and phasic contractions are generated by the ICC surrounding the myenteric plexus (ICC-MY) between the longitudinal and circular muscular layers and the ICC lining the septa separating the CM bundles (ICC-SEP). Each ICC-MY and ICC-SEP generate a spontaneous electrical slow-wave pacemaker activity that is actively propagated through the ICC network, in addition to regulating smooth muscle membrane potential and mediating enteric neurotransmission. The loss or abnormalities of ICC have been described in a variety of human motility disorders, including hypoganglionosis, Hirschsprung disease, and jejunal and ileal atresia but not in DA (29–31). A reduction in the distribution of pacemaking cells has also been reported in a dilated colon of 2 neonates with atresia of the colon (32). In the present study, we observed that the proximal segments of the obstructed site showed not only a decreased immunoreactivity to c-kit protein but also a markedly reduction in the number of ICC. The distribution of ICC also showed a discrete distribution without connection of ICC cells and a bipolar shape. This finding may be associated with the reduction of pacemaker activity and enteric neurotransmission,

thus resulting in hypoperistalsis of the proximal segments. Several physiologic studies also showed that peristalsis and spontaneous contraction were disturbed in the proximal segments. Therefore, the abnormality of ICC in the proximal segments may lead to postoperative dysmotility in DA.

In the present study, abnormalities of the enteric nerves, smooth muscle cells, and ICC were predominantly observed in the proximal segments. It has been pointed out that a tight connection existed between the ICC, enteric nervous system, and the smooth muscle to produce a synchronized and sustainable contraction of the duodenum (30). Therefore, the observed abnormalities in these 3 enteric components of the proximal duodenum suggest that duodenal motility disorders may occur later in postnatal life.

REFERENCES

1. Masumoto K, Arima T, Nakatsuji T, et al. Duodenal atresia with a deletion of midgut associated with left lung, kidney, and upper limb absences and right upper limb malformation. *J Pediatr Surg* 2003; 38:E1–4.
2. Choudhry MS, Rahman N, Boyd P, et al. Duodenal atresia: associated anomalies, prenatal diagnosis and outcome. *Pediatr Surg Int* 2009; 25:727–30.
3. Sajja SBS, Middlesworth W, Niazi M, et al. Duodenal atresia associated with proximal jejuna perforations: a case report and review of literature. *J Pediatr Surg* 2003;38:1396–8.
4. Waever E, Nielsen OH, Arnbjörnsson E, et al. Operative management of duodenal atresia. *Pediatr Surg Int* 1995;10:322–4.
5. Weber TR, Lewis E, Mooney D, et al. Dudenal atresia: a comparison of techniques of repair. *J Pediatr Surg* 1986;21:1133–6.
6. Kimura K, Mukohara N, Nishijuma E, et al. Diamond-shaped anastomosis for duodenal atresia: an experience with 44 patients over 15 years. *J Pediatr Surg* 1990;25:977–9.
7. Adzick NS, Harrison MR, deLorimier AA. Tapering duodenoplasty for megaduodenum associated with duodenal atresia. *J Pediatr Surg* 1986;21:311–2.
8. Escobar MA, Ladd AP, Grosfeld JL, et al. Duodenal atresia and stenosis: long-term follow-up over 30 years. *J Pediatr Surg* 2004;39:867–71.
9. Dalla Vecchia LK, Grosfeld JL, West KW, et al. Intestinal atresia and stenosis: a 25-year experience with 277 cases. *Arch Surg* 1998;133: 490–7.
10. Grosfeld JL, Rescorla FJ. Duodenal atresia and stenosis: reassessment of treatment and outcome based on antenatal diagnosis, pathologic variance, and long-term follow-up. *World J Surg* 1993;17:301–9.
11. Masumoto K, Suita S, Nada O, et al. Alterations of the intramural nervous distributions in a chick intestinal atresia model. *Pediatr Res* 1999;45:30–7.
12. Sai Prasad TRR, Bajpai M. Intestinal atresia. *Indian J Pediatr* 2000;67:671–8.
13. Nixon HH. Intestinal obstruction in the newborn. *Arch Dis Child* 1955;30:13–22.
14. de Lorimier AA, Harrison MR. Intestinal plication in the treatment of atresia. *J Pediatr Surg* 1983;18:734–7.
15. Takahashi A, Tomomasa T, Suzuki N, et al. The relationship between disturbed transit and dilated bowel, and manometric findings of dilated bowel in patients with duodenal atresia and stenosis. *J Pediatr Surg* 1997;32:1157–60.
16. Cezard JP, Cargill G, Faure C, et al. Duodenal manometry in postobstructive enteropathy in infants with a transient enterostomy. *J Pediatr Surg* 1993;28:1481–5.
17. Masumoto K, Suita S, Taguchi T, et al. The occurrence of unusual smooth muscle bundles expressing smooth muscle actin in human intestinal atresia. *J Pediatr Surg* 2003;38:161–6.
18. Doolin EJ, Ormsbee HS, Hill JL. Motility abnormality in intestinal atresia. *J Pediatr Surg* 1987;22:320–4.
19. Masumoto K, Suita S, Nada O, et al. Abnormalities of enteric neurons, intestinal pacemaker cells, and smooth muscle in human intestinal atresia. *J Pediatr Surg* 1999;34:1463–8.
20. Melek M, Edirne YE. Two cases of duodenal obstruction due to a congenital web. *World J Gastroenterol* 2008;14:1305–7.

21. Ando H, Kaneko K, Ito F, et al. Embryogenesis of pancreaticobiliary maljuction inferred from development of duodenal atresia. *J Hepatobiliary Pancrear Surg* 1999;1:50–4.
22. Boyden EA, Cope JG, Bill AH. Anatomy and embryology of congenital intrinsic obstruction of the duodenum. *Am J Surg* 1967;114:190–202.
23. Tepas JJ, Wyllie RG, Shermeta DW, et al. Comparison of histochemical studies of intestinal atresia in the human newborn and fetal lamb. *J Pediatr Surg* 1979;14:376–80.
24. Masumoto K, Akiyoshi J, Nagata K, et al. Chronological change in intramural components in severe proximally dilated jejuna atresia: an immunohistochemical study. *J Pediatr Gastroenterol Nutr* 2008;46: 602–6.
25. Harndy MH, Man DWK, Bain D, et al. Histochemical changes in intestinal atresia and its implications on surgical managements: a preliminary report. *J Pediatr Surg* 1986;21:17–21.
26. Pickard LR, Santoro S, Wyllie RG, et al. Histochemical studies of experimental fetal intestinal obstruction. *J Pediatr Surg* 1981;16:256–60.

27. Masumoto K, Nada O, Suita S, et al. The formation of the chick ileal muscle layers as revealed by alpha-smooth muscle actin immunohistochemistry. *Anat Embryol* 2001;201:121–9.
28. Baglaj SM, Czernik J, Kuryszko J, et al. Natural history of experimental intestinal atresia: morphological and ultrastructural study. *J Pediatr Surg* 2001;36:1428–34.
29. Jones MP, Bratten JR. Small intestinal motility. *Curr Opin Gastroenterol* 2008;24:164–72.
30. Lee HT, Hennig GW, Fleming NW, et al. The mechanism and spread of pacemaker activity through myenteric interstitial cells of Cajal in human small intestine. *Gastroenterology* 2007;132:1852–65.
31. Lee HT, Hennig GW, Fleming NW, et al. Septal interstitial cells of Cajal conduct pacemaker activity to excite muscle bundles in human jejunum. *Gastroenterology* 2007;133:907–17.
32. Sutcliffe J, King SK, Clarke MC, et al. Reduced distribution of pacemaking cells in dilated colon. *Pediatr Surg Int* 2003;23:1179–82.

— 128 —

The utility of muscle sparing axillar skin crease incision for pediatric thoracic surgery

Tomoaki Taguchi · Kouji Nagata · Yoshiaki Kinoshita · Satoshi Ieiri ·
Tatsuro Tajiri · Risa Teshiba · Genshiro Esumi · Yuji Karashima ·
Sumio Hoka · Kouji Masumoto

Abstract

Background Posterolateral or standard axillar incisions for the pediatric thoracic surgery are occasionally associated with poor motor as well as cosmetic results, including chest deformities and large surgical scars. A muscle sparing axillar skin crease incision (MSASCI) was initially proposed by Bianchi et al. (in J Pediatr Surg 33:1798–1800, 1998) followed by Kalman and Verebely (in Eur J Pediatr Surg 12:226–229, 2002) resulting in satisfactory cosmetics. However, they performed operations through the third or fourth intercostals space (ICS), therefore the target organs were restricted in the upper two-thirds of the thoracic cavity.

Patients and methods Thoracic surgeries were performed using MSASCI in 27 patients (1-day to 9-year old). There were ten patients with esophageal atresia, seven with congenital cystic adenomatoid malformation, five with pulmonary sequestration, two with mediastinal neuroblastoma, two with right diaphragmatic hernia, and one with pulmonary hypertension. A thoracotomy was performed through the appropriate ICS (from third to eighth).

Results In all patients, the expected procedures, including pulmonary lower lobectomy, were successfully performed by MSASCI throughout the thoracic cavity. A good operational field was easily obtained in neonates and infants. Most of the patients achieved excellent motor and aesthetic outcomes.

Conclusions MSASCI may become the standard approach for the thoracic surgery for small children.

Keywords Axillar skin crease · Thoracotomy · Pulmonary lobectomy · Neonate · Infant

T. Taguchi · K. Nagata · Y. Kinoshita · S. Ieiri · T. Tajiri ·
R. Teshiba · G. Esumi
Department of Pediatric Surgery, Graduate School of Medical
Sciences, Kyushu University, Fukuoka, Japan

T. Taguchi (✉)
Department of Pediatric Surgery, Reproductive and
Developmental Medicine, Faculty of Medical Sciences,
Kyushu University, 3-1-1 Maidashi, Higashi-Ku,
Fukuoka 812-8582, Japan
e-mail: taguchi@pedsurg.med.kyushu-u.ac.jp

Y. Karashima · S. Hoka
Department of Anesthesiology and Critical Care Medicine,
Graduate School of Medical Sciences, Kyushu University,
Fukuoka, Japan

K. Masumoto
Department of Thoracic, Endocrine, and Pediatric Surgery,
Fukuoka University School of Medicine, Fukuoka, Japan

Introduction

Advances in antenatal diagnosis, surgical technique and perioperative care have improved survival rate for neonatal surgical diseases. The mortality rate has become less than 10% [1]. It is now important to consider the long-term good "quality of life" (QOL) in neonatal surgical disease. Therefore, surgeons have sought to establish procedures that leave no scars, using the natural skin crease such as axillar crease and umbilical crease [2–4].

Posterolateral or standard axillar incisions for the pediatric thoracic surgery sometimes cause poor functional as well as cosmetic results, including chest deformities (scoliosis, shoulder deformity, and winged scapula) and large surgical scars. Muscle sparing axillar skin crease incision (MSASCI) was initially proposed for neonates by Bianchi et al. [5] in 1998, and then Kalman and Verebely [6] extended this approach for children in 2002, thus resulting

🖄 Springer

in a good postoperative cosmetic results. However, they performed surgery through the third or fourth intercostals space (ICS), therefore the performed operations were restricted in the upper two-thirds of the thoracic cavity.

Patients and methods

Thoracic surgeries were performed using MSASCI in 27 patients (1-day to 9-year old) from December 2006 to February 2011. There were ten patients with esophageal atresia, seven with congenital cystic adenomatoid malformation, five with pulmonary sequestration, two with mediastinal neuroblastoma, two with right diaphragmatic hernia, and one with pulmonary hypertension. The performed operations were 10 primary esophageal anastomoses, 12 pulmonary lobectomies (including lower lobectomies) or partial resections, 2 subtotal neuroblastoma resections, 1 diaphragmatic repair, 1 pulmonary biopsy, and 1 exploratory thoracotomy.

This study was performed, according to the Ethical Guidelines for Clinical Research published by the Ministry of Health, Labor, and Welfare of Japan on 30 July 2003 and complies with the Helsinki Declaration of 1975 (revised 1983). Regarding this retrospective study, properly informed consent was obtained from the parents.

The patient was placed in the lateral position. The uppermost arm was extended to about 130°, drawn forward, and placed on an arm-rest. A pulse-oxymeter was applied on hand of the extended arm.

A skin incision was made just on the axillar skin crease, and the pectoralis major and latissimus dorsi muscles were retracted superiorly and medially, respectively. Either of these muscles could be partially incised in case. The incision was deepened and the axillary fat pad and lymph nodes were pushed upward. The long thoracic nerve was preserved in the posterior part of the wound (Fig. 1). The anterior serratus muscle was split along its fibers just on the targeted costa. The thoracic cavity was entered through the appropriate ICS. The peripheral pulse was monitored by the pulse-oxymeter of the extended arm avoid a circulatory failure of the arm.

Thoracotomy for esophageal atresia was performed through the fourth ICS and the upper and lower esophagus was exposed via an extrapleural approach. After cutting The azygos vein was cut and the Tracheoesophageal fistula (TEF) was closed by 5-0 polydioxanon (PDS) transfixing sutures and cut. Esophageal end-to-end anastomosis was performed with one layer stitch sutures. Both lateral sides were approximated using 5-0 PDS, and a transanastomotic tube was inserted from the nose to the stomach through the anastomosis. The anterior and the posterior aspects were sutured with 6-0 PDS in stitch.

One-lung ventilation was attempted in order to obtain adequate operational field for pulmonary lower lobectomy [7]. Briefly, bronchial blockade with a 4Fr or 5Fr Fogarty embolectomy catheter was attempted in each case. Children were initially intubated with a Fogarty embolectomy catheter under direct laryngoscopy. Then, immediately, an endotracheal tube was placed alongside the catheter in the trachea. After securing the tube, a pediatric fiberoptic bronchoscope (2.2 mm in diameter) was passed through to set a Fogarty embolectomy catheter to the mainstem bronchus. And then, bronchial blockade was performed with its balloon inflated with an appropriate volume of normal saline. Thoracotomy was done through the fifth or sixth ICS, and then the lung was deflated. The pulmonary arteries were ligated and cut and then the bronchus was cut and closed with 5-0 PDS sutures. Finally, the pulmonary vein was doubly ligated and cut, and the pulmonary ligament was dissected.

One-lung ventilation was also performed for the pulmonary sequestration. Thoracotomy was performed via the seventh or eighth ICS in order to approach the abnormal artery in pulmonary ligament at first. One-lung ventilation allowed lower lobe to be easily lifted for the dissection of pulmonary ligament and the ligation of abnormal artery. This abnormal artery was ligated, before ligation of pulmonary vein in order to avoid lung volume expansion.

A rolled vicryl sheet was inserted between the costa during thoracic closure, in order to avoid bony adhesion in some cases. Both the thoracic and subcutaneous tubes were inserted through both ends of wound; therefore, no additional wounds were necessary for tubes.

Results

Thoracotomy was successfully done through from the third and eighth ICS using MSASCI. All of the expected procedures, including pulmonary lower lobectomies, were able to be performed adequately. A good operational field was easily obtained in neonates and infants in comparison to that in elder children. The incision was extended caudally, about 1 cm in only one infant with pulmonary sequestration. Two patients died due to the severe cardio-pulmonary anomalies, and one patient with right diaphragmatic hernia showed recurrence and required reoperation using an abdominal approach. The other patient with a right diaphragmatic hernia showed no right lung; therefore, no procedure was performed (exploratory thoracotomy).

Surgical complications included wound disruption in the four cases and transient arm paralysis in the two cases. The wound disruptions were treated by vacuum therapy and healed about 1 week, and the transient arm paralysis
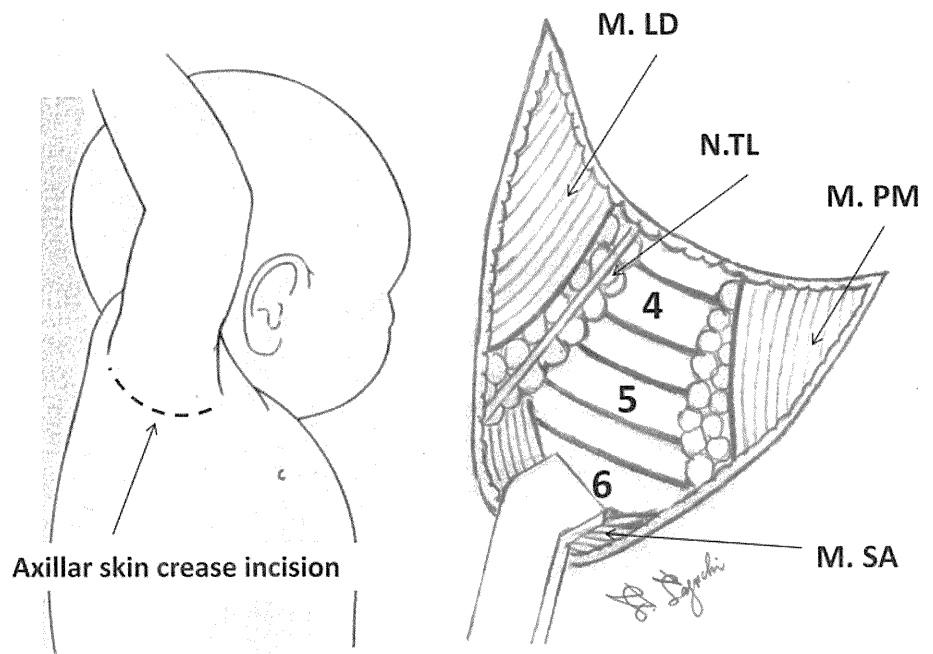
recovered spontaneously in a few weeks. All of the patients showed uneventful postoperative course and achieved excellent motor and aesthetic outcomes after 1 month. The surgical scar was almost hidden by the axillar skin crease in a year (Figs. 2, 3). So far, there have been no patients showing thoracic deformity, in a relatively short-term follow-up (no more than 4 years). The outcome of each patient is shown in Table 1.
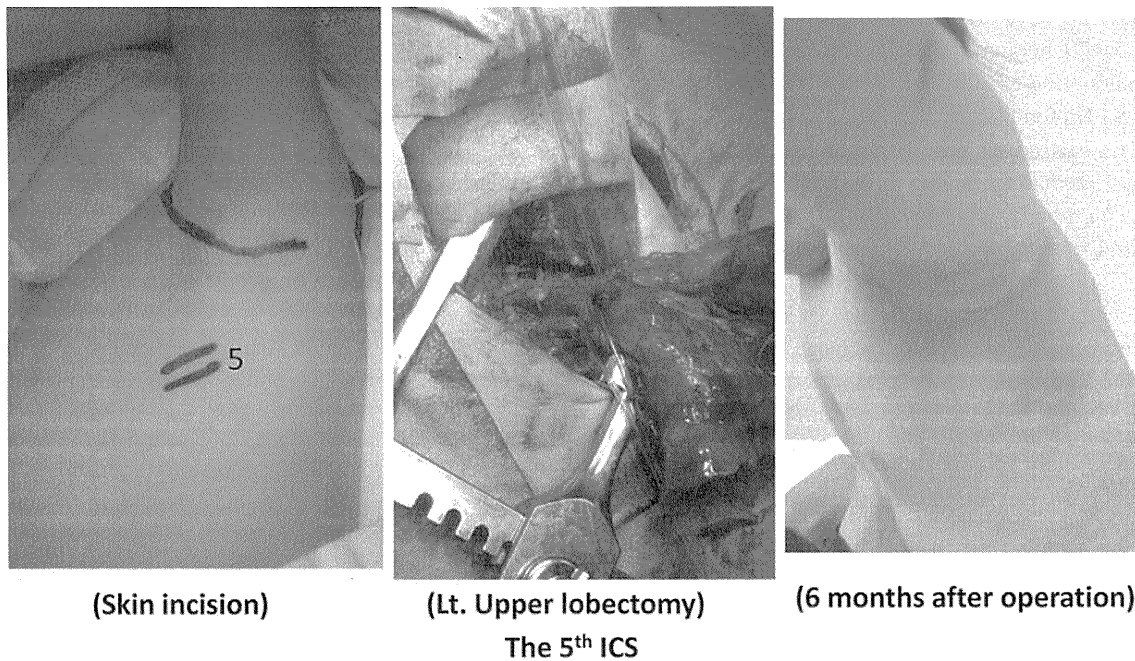

Fig. 2 Pre, intra, and postoperative appearance of Case 15. Congenital cystic adenomatoid malformation in Lt. upper lobe. *Left* skin incision on the axillar crease. *Middle* Lt. upper lobectomy of lung was performed through the fifth ICS at 1-month old. *Right* operative wound was almost hidden 6 months after operation
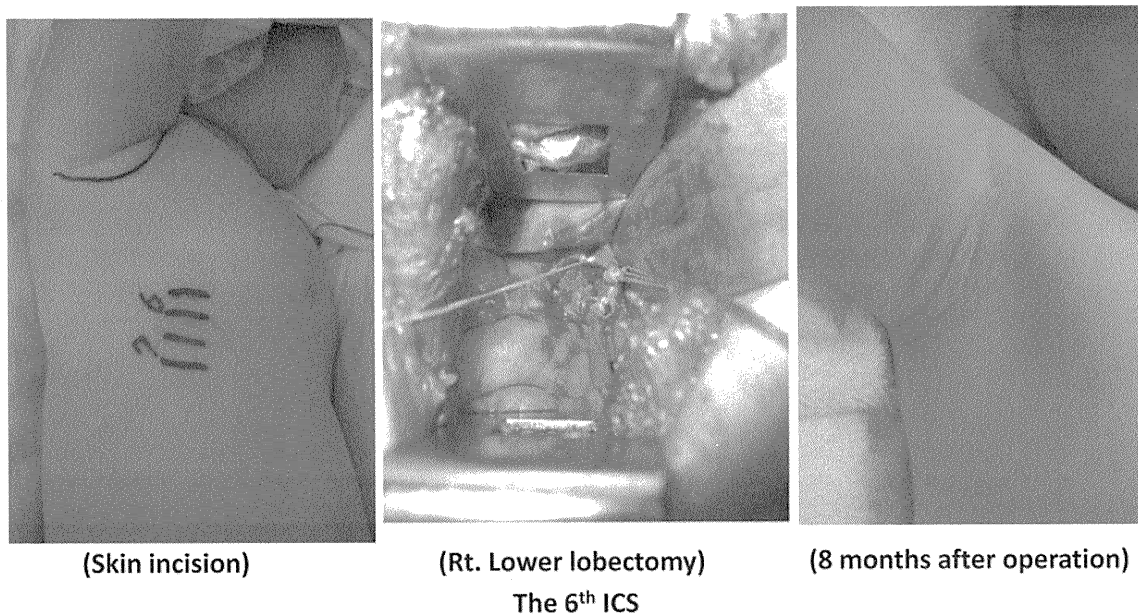
(Skin incision)   (Rt. Lower lobectomy)   (8 months after operation)

The 6th ICS

Fig. 3 Pre, intra, and post operative appearance of Case 17. Intralober lung pulmonary sequestration in Rt. lower lobe. *Left* skin incision on the axillar crease. *Middle* Rt. lower lobectomy of lung was performed through the sixth ICS at 3-month old. *Right* operative wound was almost hidden 8 months after operation

Discussion

Axillary skin crease incision for thoracic surgery was initially reported by Atkinson as "peraxillary approach" for dissection of the upper thoracic and stellate ganglia through the second ICS in adult in 1949 [8]. Bianchi et al. [5] reported using "high axillary skin crease, muscle-sparing to right lateral thoracotomy" for children in 1998. They operated on 29 neonates including 27 esophageal atresia and two patent ductus arteriosus (PDA) through the third or fourth ICS. Kalman and Verebely [6] also reported this approach as "axillary skin crease incision" for thoracotomy of neonates and children in 2002. They performed 17 operations in neonates (8 esophageal atresia, 8 PDA, 1 CCAM) and 9 operations in children (3 neuroblastoma, 1 teratoma, 5 pulmonary operations including lobectomies) through the third or fourth ICS. The oldest patient of this report was a 15-year-old girl with a large teratoma from the anterior mediastinum. They performed five pulmonary operations including one biopsy for histiocytosis, one marsupialization of an inflammatory cyst, one cystectomy of a congenital cyst and two pulmonary resections for bronchiectasia (one S2-3-4 trisegmentectomy on the left side and one middle lobe lobectomy). They concluded that it ensured unrestricted access to the upper two-thirds of the thoracic cavity through the third or fourth ICS. They did not perform any pulmonary lower lobectomies.

These reports indicate that the term MSASCI is appropriate. The approach was extended downward up to the eighth ICS in the current series to perform the expected procedures in all cases, including pulmonary lower lobectomy and intralobular pulmonary sequestration. This technique is feasible for almost all kinds of pediatric thoracic surgery from third to eighth ICS. The appropriate ICS for thoracotomy depends on the target organ. For example, the fourth ICS is used for esophageal atresia, the fifth ICS is for standard pulmonary lobectomy, and the seventh or eighth ICS for pulmonary sequestration. We experienced technical difficulties in patch closure of right diaphragmatic hernia in one case. The medial margin of diaphragmatic defect was difficult to be exposed for suturing, because liver and intestine interfered to the operation field. Right diaphragmatic hernia might not be indication for MSASCI from our restricted experience.

There were initially several complications, such as wound disruption and transient arm paralysis. In 18 out of the 27 patient, thoracotomy was performed below the fourth ICS. The wound disruption occurred in four cases (Cases 5, 7, 9 and 26). These four were operated through fifth, fourth, sixth, and fifth ICS, respectively. Three out of four cases underwent thoracotomy below the fourth ICS. Therefore, downward hyperextension of skin by metal retractor may cause wound disruption. In addition, the case five was extremely premature infant and the modified gestational age at operation was 40 weeks. Cases 7, 9 and 26 were operated in their neonatal period. And the three out of these four cases showed cyanosis in perioperative period due to their congenital heart disease and the subsequent pulmonary hypertension. Therefore, hyperextension of the skin as well as vulnerable factors of each child may cause

Table 1 Summary of 27 pediatric patients performed thoracotomies with MSASCI

Case	Sex	Diagnosis	Type or site	Age at op.	Operation	Intercostal space	Complication	Prognosis
1	M	EA	Gross type A	1 year 3 month	Esophageal EEA	Rt. 4th intercostal	Minor leakage	Alive
2	F	EA	Gross type C	2 days	Esophageal EEA	Rt. 4th intercostal	Stenosis	Alive
3	M	EA, AA, TAC	Gross type C	1 day	Esophageal EEA	Rt. 4th intercostal	None	Alive
4	F	EA	Gross type C	2 days	Esophageal EEA	Rt. 4th intercostal	None	Alive
5	F	EA, ELBWIPA stenosis	Gross type C	3 months	Esophageal EEA	Rt. 5th intercostal	TEF recurrence wound disruption	Died[b]
6	F	EA	Gross type D	1 day	Esophageal EEA	Rt. 4th intercostal	None	Alive
7	M	EA, TA	Gross type D	1 day	Esophageal EEA	Rt. 4th intercostal	Wound disruption transient paralysis	Died[c]
8	F	EA	Gross type C	1 day	Esophageal EEA	Rt. 5th intercostal	Stenosis	Alive
9	F	EA	Gross type C	1 day	Esophageal EEA	Rt. 6th intercostal	Wound disruption	Alive
10	F	EA	Gross type C	1 day	Esophageal EEA	Rt. 4th intercostal	None	Alive
11	M	CCAM	Rt. middle lobe	8 months	Partial resection	Rt. 5th intercostal	None	Alive
12	M	LPS	Rt. lower lobe	4 days	LPS resection	Rt. 5th intercostal	None	Alive
13	F	CCAM	Lt. upper lobe	1 month	Partial resection	Lt. 5th intercostal	None	Alive
14	F[a]	LPS	Lt. lower lobe	8 months	LPS resection	Lt. 8th intercostal	None	Alive
15	M	CCAM	Lt. upper lobe	1 month	Lt. upper lobectomy	Lt. 5th intercostal	Pneumothorax	Alive
16	F	CCAM	Lt. lower lobe	4 months	Lt. lower lobectomy	Lt. 5th intercostal	None	Alive
17	M	LPS	Rt. lower lobe	3 months	Rt. lower lobectomy	Rt. 6th intercostal	None	Alive
18	F	CTA with LPS	Lt. lower lobe	4 months	Rt. lower lobectomy	Rt. 6th intercostal	Transient paralysis	Alive
19	M	CCAM	Lt. lower lobe	3 months	Lt. lower lobectomy	Lt. 6th intercostal	None	Alive
20	M	CCAM	Rt. lower lobe	4 months	Rt. lower lobectomy	Rt. 5th intercostal	None	Alive
21	M	LPS	Lt. lower lobe	7 months	LPS resection	Lt. 7th intercostal	None	Alive
22	F	CCAM	Rt. lower lobe	4 months	Rt. lower lobectomy	Lt. 5th intercostal	None	Alive
23	M	Mediastinal NB	Lt. upper lobe	6 years 1 month	Subtotal excision	Lt. 4th intercostal	None	Alive
24	F	Mediastinal NB	Lt. upper lobe	9 years 4 months	Subtotal excision	Lt. 3th Intercostal	None	Alive
25	M	Pulmonary HT	Lt. upper lobe	5 years 11 months	Biopsy	Lt. 6th intercostal	None	Alive
26	M	Rt. CDH		5 days	Repair	Rt. 5th intercostal	Wound disruption CDH recurrence	Alive
27	F	Rt. CDH Rt. lung agenesis		5 days	Exploratory thoracotomy	Rt. 7th intercostal	None	Alive

EA esophageal atresia, *AA* anal atresia, *TAC* truncus arteriosus communis, *ELBW* extremely low birth weight infant, *PA* pulmonary artery, *TA* tricuspid atresia, *CCAM* congenital cystic adenomatoid malformation, *LPS* lung pulmonary sequestration, *CTA* congenital tracheal atresia, *NB* neuroblastoma, *CDH* congenital diaphragmatic hernia, *HT* hypertension, *EEA* end to end anastomosis, *TEF* tracheoesophageal fistula

[a] Incision was extended caudally about 1 cm

[b, c] Two patients died due to the severe cardio-pulmonary anomalies

the wound disruption. In order to prevent this complication, a wound retractor XS has been currently applied to protect the surgical wound. This instrument can prohibit skin and subcutaneous tissue damage during surgery. Postoperative subcutaneous negative-pressure drainage is also an effective for avoiding or treating wound disruption.

The transient arm paralysis occurred in the case 7 and 18. They were operated through the fourth ICS and the sixth ICS, respectively. Therefore, the transient paralysis is not considered to be related to the level of thoracotomy. Actually, there were no complications in the patients operated from the seventh to eighth ICS. Currently, a pulse-oxymeter has been applied, on the hand, of the extended arm for monitoring peripheral blood pulse and saturation of oxygen. During operation blood pulse and saturation of oxygen has been kept in normal range. Since then, no patient has experienced transient arm paralysis. Therefore, transient arm paralysis is considered to be vascular origin caused by the hyperextension of arm or the hyperextension of wound.

The surgical field is relatively small; therefore, there are a few technical methods in order to overcome this disadvantage. One-lung ventilation is required for pulmonary lower lobectomy during the dissection of the pulmonary ligament and pulmonary vein. Furthermore, one-lung ventilation provides adequate operative field in ligation of the abnormal artery during surgery of pulmonary sequestration. One-lung ventilation has been technically feasible in infant, using Fogarty embolectomy catheter [7]. Hemoclips facilitate the ligation of pulmonary arteries. The proximal site is ligated by 3-0 or 4-0 silk suture and the distal site is closed by a hemoclip, to provide sufficient distance for a safe cut. A long and fine-tip needle holder and forceps are required for dissection of the TEF and anastomosis of the esophagus in esophageal atresia. Fine monofilament absorbable 5-0 or 6-0 PDS with the two needles in both ends are useful for full thickness stitch suture using an inside-to-outside and inside-to-outside manner.

In conclusions, MSASCI for pediatric thoracic surgery resulted in excellent motor and aesthetic outcomes. MSASCI may become the standard approach for thoracic surgery for the small children, especially for neonates and infants.

References

1. Taguchi T (2008) Current progress in neonatal surgery. Surg Today 38:379–389
2. Taguchi T (2008) Scar less surgery and reconstructive surgery in neonates (Plenary Lecture 7). In: 15th congress of the federation of Asia and oceania perinatal societies, 20th–24th May 2008, Program & Abstract pp 69–70
3. Tajiri T, Ieiri S, Kinoshita Y, Masumoto K, Nishimoto Y, Taguchi T (2008) Transumbilical approach for neonatal surgical diseases: woundless operation. Pediatr Surg Int 24:1123–1126
4. Takahashi Y, Tajiri T, Masumoto K, Kinoshita Y, Ieiri S, Matsuura T, Higashi M, Taguchi T (2010) Umbilical crease incision for duodenal atresia achieves excellent cosmetic results. Pediatr Surg Int 26:963–966
5. Bianchi A, Sowande O, Alizai NK, Rampersad B (1998) Aesthetics and lateral thoracotomy in the neonate. J Pediatr Surg 33:1798–1800
6. Kalman A, Verebely T (2002) The use of axillary skin crease incision for thoracotomies of neonates and children. Eur J Pediatr Surg 12:226–229
7. Camci E, Tuğrul M, Tuğrul ST et al (2001) Techniques and complications of one-lung ventilation in children with suppurative lung disease: experience in 15 cases. J Cardiothorac Vasc Anesth 15:341–345
8. Atkins HJB (1949) Peraxillary approach to the stellate and upper thoracic sympathetic ganglia. The Lancet 254:1152